6-17-2010

Generation of Tunable Narrow Bandwidth Nanosecond Pulses in the Deep Ultraviolet for Efficient Optical Pumping and High Resolution Spectroscopy

Luis Velarde
University of California, Santa Barbara

Daniel P. Engelhart
University of California, Santa Barbara

Daniel Matsiev
University of California, Santa Barbara

Jerry L. LaRue
Chapman University, larue@chapman.edu

Daniel J. Auerbach
University of California, Santa Barbara

See next page for additional authors

Recommended Citation

L. Verlarde, P. Engelhart, D. Matsiev, J. LaRue, D. J. Auerbach, A. M. Wodtke, Generation of tunable narrow bandwidth nanosecond pulses in the deep-ultraviolet for efficient optical pumping and high resolution spectroscopy, *Rev. Sci. Instrum.* 2010, 81, 063106, DOI: 10.1063/1.3436973

Generation of Tunable Narrow Bandwidth Nanosecond Pulses in the Deep Ultraviolet for Efficient Optical Pumping and High Resolution Spectroscopy

The following article appeared in

L. Verlarde, P. Engelhart, D. Matsiev, J. LaRue, D. J. Auerbach, A. M. Wodtke, Generation of tunable narrow bandwidth nanosecond pulses in the deep-ultraviolet for efficient optical pumping and high resolution spectroscopy, *Rev. Sci. Instrum.* 2010, 81, 063106, DOI: 10.1063/1.3436973

and may be found at DOI: 10.1063/1.3436973.

Authors

Luis Velarde, Daniel P. Engelhart, Daniel Matsiev, Jerry L. LaRue, Daniel J. Auerbach, and Alec M. Wodtke

Generation of tunable narrow bandwidth nanosecond pulses in the deep ultraviolet for efficient optical pumping and high resolution spectroscopy

Luis Velarde,[1] Daniel P. Engelhart,[1] Daniel Matsiev,[1] Jerry LaRue,[1] Daniel J. Auerbach,[1,2] and Alec M. Wodtke[1,a)]
[1]*Department of Chemistry and Biochemistry, University of California, Santa Barbara, California 93106, USA*
[2]*Gas Reaction Technologies, 861 Ward Drive, Santa Barbara, California 93111, USA*

(Received 22 April 2010; accepted 6 May 2010; published online 17 June 2010)

Nanosecond optical pulses with high power and spectral brightness in the deep ultraviolet (UV) region have been produced by sum frequency mixing of nearly transform-limited-bandwidth IR light originating from a home-built injection-seeded ring cavity $KTiOPO_4$ optical parametric oscillator (OPO) and the fourth harmonic beam of an injection-seeded Nd:YAG laser used simultaneously to pump the OPO with the second harmonic. We demonstrate UV output, tunable from 204 to 207 nm, which exhibits pulse energies up to 5 mJ with a bandwidth better than 0.01 cm^{-1}. We describe how the approach shown in this paper can be extended to wavelengths shorter than 185 nm. The injection-seeded OPO provides high conversion efficiency (>40% overall energy conversion) and superior beam quality required for highly efficient downstream mixing where sum frequencies are generated in the UV. The frequency stability of the system is excellent, making it highly suitable for optical pumping. We demonstrate high resolution spectroscopy as well as optical pumping using laser-induced fluorescence and stimulated emission pumping, respectively, in supersonic pulsed molecular beams of nitric oxide. © *2010 American Institute of Physics.*
[doi:10.1063/1.3436973]

I. INTRODUCTION

An all-solid-state tunable source of coherent ultraviolet (UV) radiation with high peak power and narrow bandwidth is highly desirable for a number of spectroscopic and photochemical applications.[1,2] Such a source would be especially attractive when exhibiting robust long-lived performance, overall simplicity, and wide wavelength tunability with Fourier transform (FT) limited bandwidth. For pulses of nanosecond duration, the FT limit allows exceptionally narrow bandwidths to be obtained. While achieving a narrow linewidth is essential to high-resolution laser spectroscopy, high spectral brightness with long-term wavelength stability is needed for many molecular optical pumping processes, particularly in demanding spin-forbidden transitions to metastable states.[3–7] The use of tunable infrared (IR) and visible lasers to generate UV radiation by means of nonlinear frequency conversion methods remains the standard approach to producing tunable UV light. Dye lasers have been used for decades as the primary source of tunable pulsed visible and near-IR light due to their high lasing efficiency and broad tuning ranges. For FT-limited pulse generation, pulse-amplified ring dye lasers have been commonly used due to their ability to operate on a single longitudinal mode (SLM) with high powers.[8–12] To overcome the disadvantages of dye laser systems, such as poor beam quality, short-lived dye solutions, amplified spontaneous emission, and toxic chemicals, pulsed all-solid-state tunable UV sources have been proposed and developed in which the FT limit is attained via injection seeding of, for example, Ti:sapphire amplifiers (Refs. 13–15 and references therein) and optical parametric oscillators (OPOs) (e.g., Refs. 1, 16, and 17). Other methods involving intracavity elements such as etalons (e.g., Ref. 18) and grazing-incidence gratings[19,20] have also been used. Unfortunately, all of these narrow-band UV systems have a relatively high degree of complexity or rather low output powers. Intracavity sum frequency mixing has been proposed by Fix and Ehret,[21] where conversion efficiency was reported to be twice as much as external mixing. Armstrong and Smith performed intracavity mixing in an injection-seeded OPO. They postulated that absorption heating in the β-barium borate (BBO) sum frequency generation (SFG) crystal caused some signal wavefront distortion after repeatedly passing through the heated BBO, reducing the beam quality and causing hot spots in the UV output.[17] Implementing intracavity SFG in the deep UV is further complicated by absorption in transmissive outcoupling and by the high demands on the optical coatings of the resonator mirrors requiring multiple wavelength optimization (i.e., pump, signal, idler, and UV).

Inspired by recent developments in high performance injection-seeded nanosecond OPOs[1,2,16,22–30] combined with remarkable improvements in the tunability and long-term stability of diode lasers, our approach uses a mid-IR OPO, where FT-limited pulses can be readily obtained by injection seeding with a low power SLM diode laser. Subsequently,

a)Electronic mail: wodtke@chem.ucsb.edu.

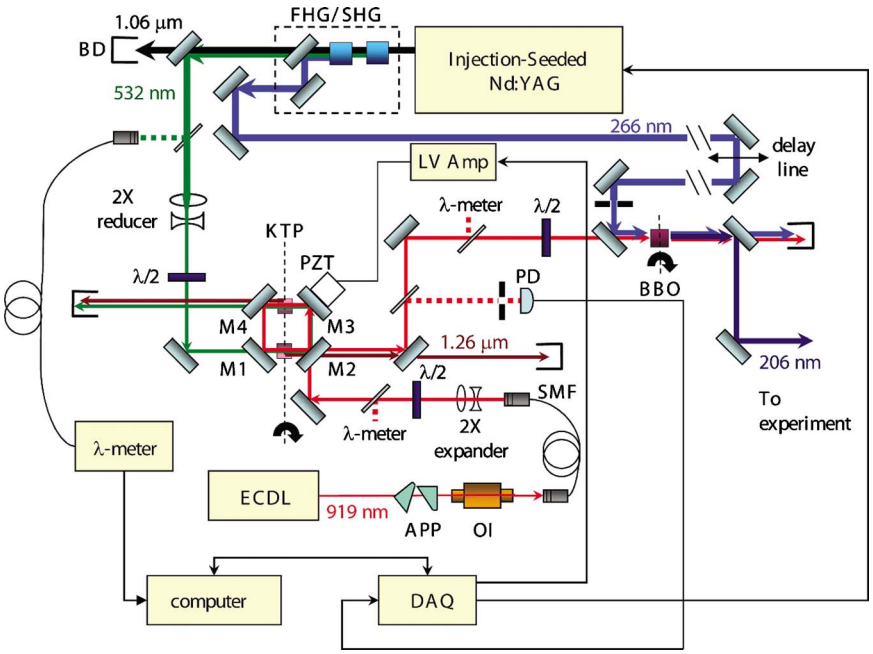

FIG. 1. (Color online) Optical layout of the injection-seeded OPO and the frequency locking setup. ECDL =external cavity diode laser, DAQ =data acquisition card, PZT =piezoelectric transducer, BD=beam dump, OI=optical isolator, APP =anamorphic prism pair, PD =photodiode, SMF=single mode fiber, and LV Amp=low voltage amplifier.

frequency upconversion is accomplished by mixing the mid-IR OPO output with the fourth harmonic of an injection-seeded Nd:yttrium aluminum garnet (YAG) laser, which is concurrently used to pump the OPO with the residual second harmonic.

The general design of the OPO is based on the recent work of Mahnke *et al.*,[29] where an IR light source for atmospheric remote sensing was demonstrated. In this work we introduce a number of refinements and simplifications to the Mahnke design to function as a spectroscopic tool and demonstrate operation in the deep UV. To stabilize the OPO cavity length and lock it to the diode laser, a new simplified implementation of the intensity-dip locking method[31] was developed using merely a photodiode (PD) and a low-cost general purpose data acquisition (DAQ) card as discussed in Sec. II C.

A significant increase in the efficiency of the sum frequency mixing process is observed upon injection seeding of the OPO, demonstrating one of the advantages of the improved beam properties of the seeded near-IR source. With our current setup, the 875–940 nm FT-limited tuning range of the OPO (limited by the seed laser) generates narrow-band UV pulses in the 204–207 nm range after the SFG stage. The linewidth of the deep-UV radiation generated by this laser system is determined by laser-induced fluorescence (LIF) spectroscopy of nitric oxide. We also demonstrate the utility of the light source in optical pumping taking advantage of its excellent long term wavelength stability.

II. EXPERIMENTAL SETUP

A. Injection-seeded OPO

The optical layout of the UV light source is shown in Fig. 1. The OPO is pumped by the second harmonic (532 nm) of a *Q*-switched injection-seeded Nd:YAG laser (Spectra Physics LAB-70-10, flashlamp pumped at a repetition rate of 10 Hz, which provides single-longitudinal and single-transverse mode output with an approximately flat-topped transverse intensity profile. Pumping the OPO with 532 nm light is preferred over a 355 or 266 nm pump not only for the reason that it facilitates production of near-IR radiation needed for our SFG scheme, but also because higher energies are available at 532 nm, and optical components with higher damage threshold can be readily obtained. This scheme employing a 532 nm pump pulse provides higher levels of safety, as the most dangerous laser beam is always visible to the user. Pulse energies up to 140 mJ are available at 532 nm when 70 mJ of 266 nm are simultaneously produced. A pulse duration of 8–9 ns full width at half maximum (FWHM) was typically observed for the fundamental and ~7.5 and ~6 ns for the second and fourth harmonics, respectively. The pump beam diameter is reduced to 4–5 mm by means of a telescope (Special Optics, Inc.). Single-mode operation of the OPO was achieved by means of injection seeding with a cw single-frequency diode laser tuned to the signal frequency. An external cavity diode laser (ECDL) provided up to 18 mW of cw SLM light (Toptica Photonics, Inc. DL Pro 895) at the output of a single-mode polarization-maintaining optical fiber. The ECDL tuning range is 875–940 nm with a continuous, mode-hop-free, scanning range of approximately 20 GHz. Typically, 2–5 mW were used for injection seeding. This power allows for the beam diameter of the diode laser to be expanded to ~4.5 mm (Thorlabs, Inc. BE02M-B) or slightly larger than the pump diameter to allow for maximum spatial overlap of the carefully collimated beams.

The overall design of the signal-resonant OPO is based on the previous work of Mahnke *et al.*[29] The optical resonator is built to allow oscillation of the signal wavelength and consists of a piezoelectrically tuned four-mirror planar ring cavity. Custom mirrors (Laser Optik, GmbH) are needed for this cavity as are shown in Fig. 2. A pair of identical nonlinear KTP ($KTiOPO_4$) crystals are placed inside the cavity in a walkoff compensated configuration.[32] The resonator is formed by mirrors M1 to M4, where M2 is the output coupler (OC) and M3 is placed on a stacked ring piezoelectric

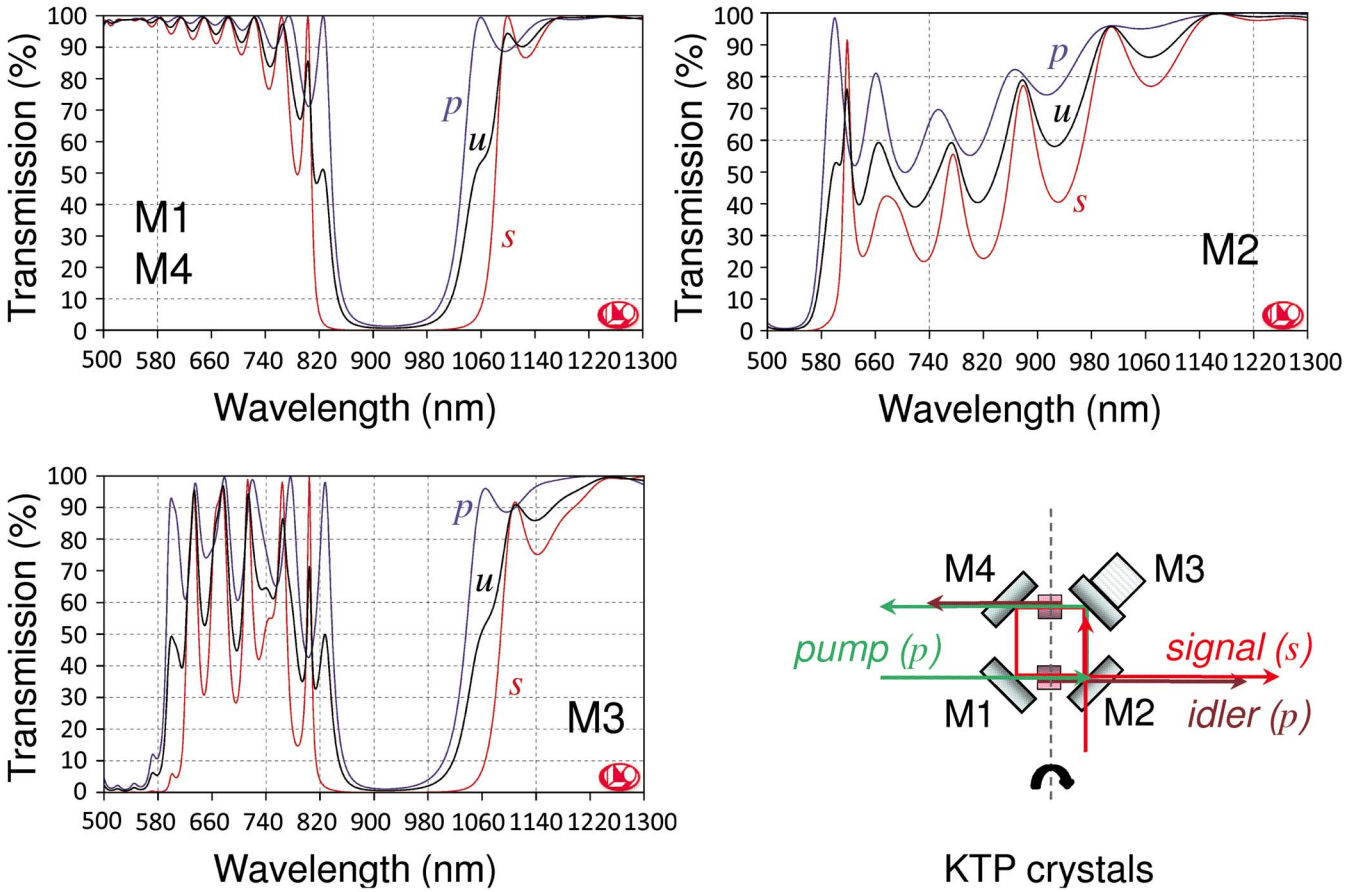

FIG. 2. (Color online) Transmission curves (shown with permission from Laseroptik, GmbH) for the OPO cavity mirrors for p (upper traces), s (lower traces), and unpolarized (middle traces) light, where p indicates polarization parallel and s indicates polarization perpendicular (senkrecht) to the plane in which the light travels in the cavity. The mirrors are coated for a 45° incidence angle.

transducer (PZT) (Piezomechanik, GmbH, HPSt 150/20–15/12 VS35) to actively stabilize the cavity length. Details of the stabilization feedback loop are described below in Sec. II C. The OC is coated for high reflectivity at 532 nm, high transmission for the idler, and 40%–60% reflectivity in the wavelength range of the seeder (875–950 nm). The 532 nm pump pulse enters the cavity through mirror M1 and exits through mirror M4 after making a single pass through both nonlinear crystals. In this design, the idler is dumped between crystals through mirrors M2 and M4 to prevent a fixed phase relationship of the OPO beams at the next crystal and to avoid back conversion.[29] The design has the further advantage that no optical isolator is needed between OPO and pump source. All mirrors are flat with a 1 in. diameter. Each arm of the resonator is 4.5 cm long, limited by the size of the current mirror and crystal mounts. The resulting optical length of the cavity is approximately 19 cm, with a free spectral range (FSR) of 1.58 GHz.

The KTP crystals (Newlight Photonics, Inc.) are flux grown, 10 mm long, with an 8×8 mm^2 aperture that has a protective (P-type) coating[33] with reflectivity minimized for the signal and pump wavelengths (<1%). Figure 3 shows angle tuning results from the nonlinear modeling SNLO program.[34] The crystals are cut in the XZ plane ($\varphi=0°$) with $\theta=70°$, where θ is the polar angle measured with respect to the crystalline Z axis and φ is the azimuth angle with respect to X in the XY plane. Type-II collinear phase matching occurs with an e-polarized signal and o-polarized pump and idler ($o\rightarrow o+e$). The o-polarization direction in the crystals is parallel to the Y axis and the e-polarization direction lies in the XZ plane as shown in Fig. 3. The crystals are oriented

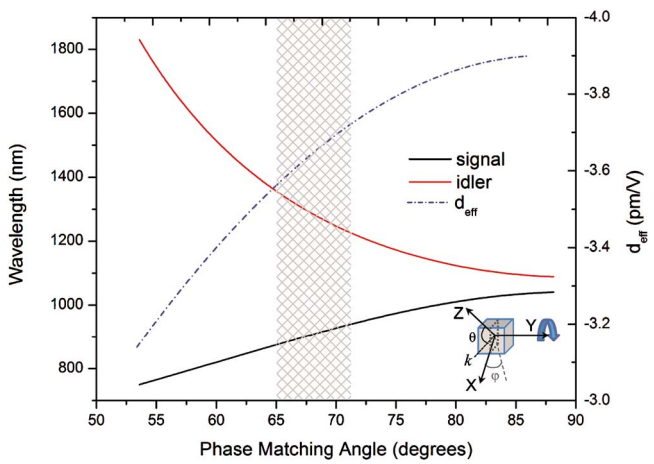

FIG. 3. (Color online) Nonlinear properties of KTP crystals cut in the XZ plane as simulated with the SNLO program (Ref. 34). The solid lines are the signal (upper solid) and idler (lower solid) wavelengths for phase-matched conditions. The scale on the right vertical axis applies to the effective nonlinear coefficient (d_{eff}) shown in the dot-dashed line. The shaded area corresponds to the tuning capabilities of the ECDL seed laser used in this work. The phase-matching angle (θ) is shown pictorially in the bottom right corner, where k is the light propagation direction.

such that the signal has *s* polarization with respect to the cavity mirrors in order to take advantage of the higher tunability range of the coatings for *s* polarization. This comes somewhat at the expense of a smaller reflectivity of the mirrors for the *p*-polarized 532 nm pump (99%). Tuning of the OPO was accomplished by rotating the crystals around the *Y* axis by separate piezomotor-driven rotation stages (Newport Corp. AG-PR100) while keeping the angle φ at 0°. The acceptance angles for each 1 cm KTP crystal are on the order of 1.4 and 2.0 mrad for the signal and idler, respectively, as obtained from simulations performed with the SNLO software.[34]

In brief, an optical parametric process consists of a pump beam ω_{pump} which is "split" by a nonlinear process that is the time reversal of sum frequency generation into a signal ω_{signal} and an idler ω_{idler} beam such that $\omega_{\text{pump}}=\omega_{\text{signal}}+\omega_{\text{idler}}$ and $\omega_{\text{signal}}>\omega_{\text{idler}}$. The electric fields $E(\omega_{\text{signal}}), E(\omega_{\text{idler}})$ of the signal and idler waves produced by the nonlinear polarization $P(\omega_{\text{pump}})$ generated in phase with the pump electric field $E(\omega_{\text{pump}})$ are coupled by means of the second-order polarizabilty tensor. For our fixed geometry, this coupling can be simply described by the scalar relation $P(\omega_{\text{pump}}) \propto d_{\text{eff}} E(\omega_{\text{signal}}) E(\omega_{\text{idler}})$, where the KTP effective nonlinear coefficient[35] $d_{\text{eff}}=d_{32} \sin\theta$ is directly related to the parametric gain and calculated to be about -3.6 pm/V for wavelengths in our tuning range. This is shown in Fig. 3 along with the calculated phase matching curves for parametric conversion in 532 nm pumped KTP.[34] The signal on the free-running (unseeded) OPO could be experimentally tuned around 830–990 nm as measured with a grating spectrometer (Ocean Optics, Inc.). Beyond these limits, the OPO output becomes severely impaired as a result of the reduced reflectivity of the OPO cavity mirrors and the walkoff induced by the increased crystal angles.

B. Generation of narrow-band deep-UV pulses

While the OPO is pumped by the second harmonic of an injection-seeded Nd:YAG laser, up to 70 mJ of 266 nm light can be produced simultaneously as schematically shown in Fig. 1. To minimize optical damage, an aperture is used to select only about 10 mJ of the 266 nm beam with the most homogenous beam profile possible, which is then mixed in a BBO crystal (Castech, Inc.) with the tunable FT-limited output of the OPO to generate pulses in the 204–207 nm range. An optical delay line is introduced to the path of the *p*-polarized 266 nm light to achieve temporal overlap at the mixing crystal with the OPO signal pulse. A $\lambda/2$ waveplate is used to adjust the polarization of the OPO to match that of the 266 nm beam. An uncoated 10 mm long BBO crystal with an aperture of 7×7 mm^2 and cut at $\theta=56°$ with respect to the crystal axis is used for type-I phase matching ($o+o\rightarrow e$). While the walkoff angle is large, close to 90 mrad, and acceptance angles are small, 0.61 and 0.17 mrad for the IR and UV beams, respectively, the $d_{\text{eff}}=1.7$ pm/V proves to be superior to type-II mixing (0.3 pm/V).[34] The deep-UV beam can be separated from the other wavelengths by the use of a low-pass dichroic mirror or a Pellin–Broca prism.

Performance characteristics required for efficient nonlinear frequency mixing include high pulse energy, narrow linewidth, low beam divergence, reduced jitter, and mutual coherence of the interacting pulses. In this logic, the enhanced properties of the injection-seeded OPO beam are expected to positively impact the efficiency of the mixing process.

C. OPO cavity locking and frequency stabilization

Although one generally needs only a moderate optical power to be injected into one of the OPO axial modes to achieve injection seeding, this is best accomplished when the cavity length is matched to be a multiple of the injected wavelength. Deviations from an exact match affect the conversion efficiency and introduce discrepancies between output and seeding frequencies.[36] Hence, stable long-term FT-limited operation of the OPO requires active stabilization of the cavity length to compensate for optical, mechanical, or thermal drifts and fluctuations. Additionally, in order to perform continuous wavelength scans with SLM quality, it is generally necessary to establish a feedback servo loop to allow the cavity length to follow the scanning injection-seeding wavelength. Conveniently, no angular adjustments of the OPO (KTP) crystals were necessary in order to cover the continuous, mode-hop-free, 20 GHz tuning range of our cw diode injection-seed laser. However, larger wavelength changes do require adjustments of the KTP crystals so that the center of the phase-matched OPO gain profile will be positioned near the seeded mode. In general, a minimal frequency chirp is obtained when the seeder wavelength equals the free-running wavelength of the phase-matched OPO.[37,38] It has been experimentally observed that for a large phase mismatch (seed laser detuning) it becomes more challenging to seed the OPO and achieve a high spectral purity.[29,39,40]

Several well-established schemes for resonator length stabilization, such as Hänsch–Couillaud[41] and Pound–Drever–Hall,[42] have been applied to injection-seeded systems. These schemes derive the error signal from the cw light reflected off by the cavity, usually much weaker than the high-power pulsed OPO output, which may cause saturation (and sometimes damage) in the PDs and locking electronics if no additional precautions are taken. Other stabilization methods are able to derive the error signal directly from the pulsed OPO output, such as minimizing the buildup time[43] and the dither-and-lock technique.[22] The buildup time for nanosecond pulses in OPOs is typically a fraction of the pump pulse duration; therefore minimizing the buildup time demands fast and sensitive electronics, making the technique less attractive for these systems. The dither-and-lock method is robust and has been widely applied to many injection-seeded OPOs. It requires fast dithering of the cavity and somewhat complicated phase sensitive detection. Other more recent schemes involve optical heterodyning of the seeder and pulsed OPO radiation[36] or hybrid techniques such as the "intensity-dip" method of He and Orr.[31] Another novel stabilization method that offers dual-wavelength capability employs a sine-offset control and synchronous fire scheme.[44]

Initially, we adopted the scheme of Hänsch and Couillaud using the birefringence of the nonlinear crystals to derive the locking signal by polarization difference analysis of the light reflected by the cavity. While excellent performance

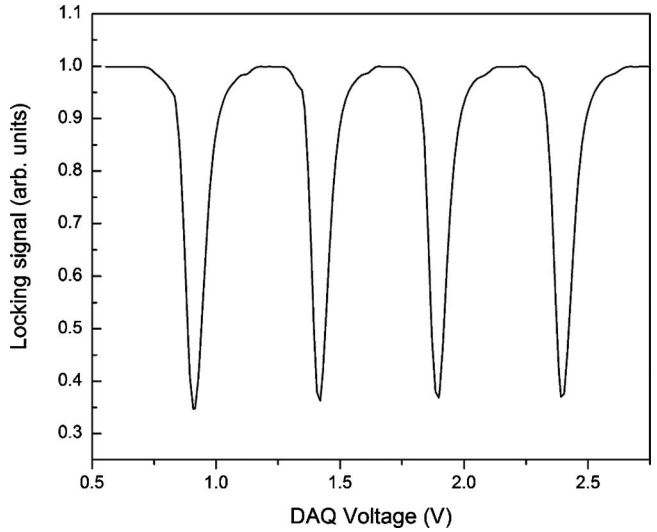

FIG. 4. Cavity fringes of the OPO ring cavity observed as the PZT element on mirror M3 is scanned. The DAQ voltage is amplified ~18× before it reaches the piezoelement. Each dip corresponds to a resonant configuration of the resonator with respect to the injected seed wavelength.

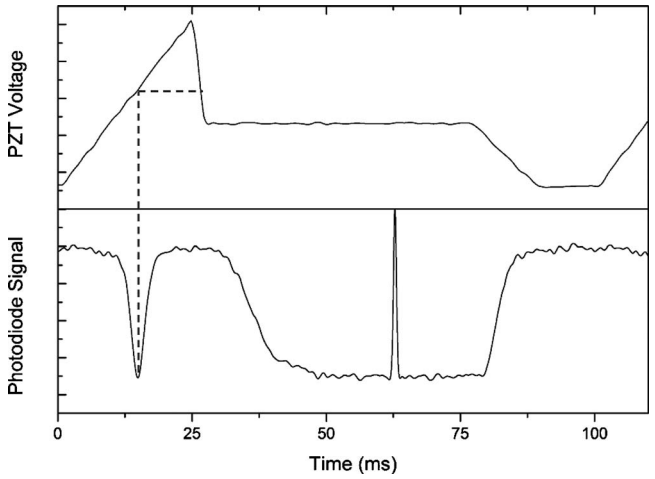

FIG. 5. Ramp, hold, and fire locking scheme. Upper trace: piezovoltage; lower trace: PD signal. The discrepancy (indicated by the dashed curve) between the "found" PZT voltage corresponding to the dip in the PD signal and the "hold" voltage where the pump fires is attributed to hysteresis of the piezo and is accounted for in the locking software.

was achieved when only the cw laser was circulating through the cavity, laborious effort was necessary to achieve long-term stability of the error signal during the high power pulsed operation. Although we did not study this effect in detail, we believe that problems arise from thermal drift in the crystals' birefringence induced by the high power pump beam.

We found that a variation in the intensity dip method worked best for our needs.[31] As the cavity length is swept by ramping the PZT voltage, one may observe that the signal from a PD monitoring the overall reflected cw light from the resonator exhibits a series of well-defined dips corresponding to the cavity length being resonant with the seeding wavelength (see Fig. 4). The depth of modulation is typically 40%–65%, depending on intracavity losses at a particular wavelength. It was experimentally verified that these dips coincide with the maximum output power of the OPO, as well as the maximum injection efficiency of the cw diode laser. By implementing a locking scheme to hold the cavity at a position which minimizes this reflection, we were able to obtain active cavity locking to the seed laser wavelength. Specifically, the intensity of cw light reflected by the OPO cavity is continuously monitored by a PD (Thorlabs, Inc. DET100A) and the PZT position which produces the dip in the intensity of the reflected beam is located by a "sweep, hold, and fire" sequence (see Fig. 5).

First, a trigger pulse from a delay generator (SRS, Inc. DG535) is sent to a low-cost DAQ card (National Instruments Corp. NI PCI-6025E) on our control computer to start the locking cycle (Fig. 5). The computer then sweeps the PZT voltage across a fringe, while the PD signal is simultaneously recorded using the DAQ unit, allowing the determination of the PZT voltage which corresponds to the reflection minimum. An aperture is used to limit the amount of light reaching the PD, which has a large area and a moderate damage threshold. The DAQ card also provides the ramp voltages necessary to sweep the PZT element. A low voltage amplifier (0–30×, −30–150 V, Piezomechanik, GmbH SVR 150/1) was used between the low-pass filtered DAQ output and the PZT. The passive home-built low-pass filter is used to extend the lifetime of the PZT as it has a cutoff frequency of 5 kHz, well below the mechanical resonance frequency of the PZT. After this sweep, the PZT voltage is adjusted back to the value producing the reflection minimum and that voltage is held for a few milliseconds. The pump laser is then fired and finally the PZT is reset to its initial preset value where the loop starts again and is repeated at the repetition rate of the laser (10 Hz).

A subtle advantage to this approach is the avoidance of any need to apply high voltages to the PZT to perform wide seed-laser scans. Since the PZT is always reset to the same initial value, the ramp, hold, and fire technique always locks to the nearest cavity mode.

The locking scheme is conveniently implemented in LabVIEW™ (National Instruments Corp.) and the program diagram is attached as supplementary material.[45] A nice feature of this routine results from the fact that we continuously monitor the cw light during PZT ramping, effectively using the OPO cavity as a diagnostic low-resolution scanning Fabry–Pérot interferometer.

In practice, there is a small (~15%) hysteresis in the PZT motion which is found upon moving back to the "hold position." While a more expensive PZT element with higher linearity and reduced hysteresis could have been purchased, an empirically determined correction factor in the LabVIEW™ program worked very well to compensate for servo loop hysteresis.

Long term wavelength drifts of the pump Nd:YAG laser were compensated using another LabVIEW™ programed locking algorithm that read the output of a high precision pulsed wavemeter (HighFinesse WS7) and used this reading to lock to a predetermined wavelength. The idea is based on the work of Kobtsev *et al.*[46] The wavemeter readout is averaged for a few laser shots and the result is compared to the predetermined set-point wavelength. Applying a small cor-

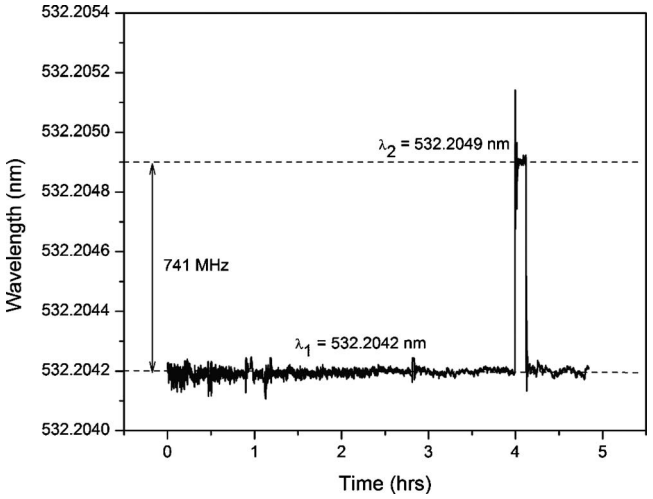

FIG. 6. Stabilization of the injection-seeded Nd:YAG laser by a wavemeter. At $t=0$, the laser was turned on without previous warming and set to lock at λ_1. Notice how after ~2.5 h narrower traces are seen indicating that the full warmup time of the laser has finished. At about 4 h, the set point in the locking program is changed to λ_2 in order to illustrate the technique, then it is brought down to the initial set point λ_1.

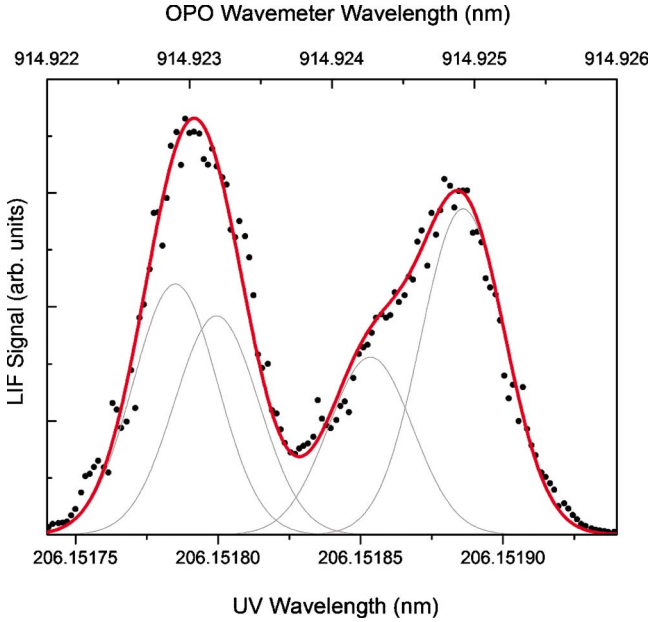

FIG. 7. (Color online) Representative LIF spectrum obtained from the $R_{11}(0.5)$ $B\,^2\Pi_{1/2}$ $(v=3)\leftarrow X\,^2\Pi_{1/2}$ $(v=0)$ rotational transition. The spectrum clearly shows Λ doubling and partially resolved hyperfine structure, which is fitted by individual Gaussian curves of 250 MHz FWHM.

recting voltage to the frequency offset input of the injection-seeding system of the Nd:YAG laser returns the laser to the set point. Figure 6 shows the wavelength stability obtained in this way. The same algorithm was successfully applied to stabilize the seeder ECDL within the resolution of the wavemeter (100 MHz). While both lasers can be stabilized simultaneously, a dual-input capability on the wavemeter is required.

III. SYSTEM PERFORMANCE

In this section, we present a variety of observations reflecting the performance of the OPO based UV light source described above. We first present in Sec. III A "real world" examples of uses of the system, namely, recording of the LIF spectrum of a molecular-beam-cooled sample as well as an application in optical pumping. In Sec. III B we present more detailed diagnostic measurements of the OPO and summarize important optical parameters such as conversion efficiency and linewidth.

A. Applications to high resolution spectroscopy and optical pumping

The deep-UV light source described in this work is well suited to applications in optical pumping and high resolution spectroscopy. To demonstrate this, we chose nitric oxide (NO) as a test molecule based on existing know-how in our group.[10,47–50] The molecular beam apparatus is described elsewhere.[48–50] In brief, a gas mixture of 5% NO in Kr is expanded into vacuum by means of a home-built pulsed piezoelectric valve (1 mm expansion orifice) to create a supersonic molecular beam of rotationally cold NO molecules. The beam passes through a 2 mm diameter collimating skimmer (Beam Dynamics, Inc.) placed 3 cm from the nozzle, into a differentially pumped region where it is crossed orthogonally by the UV light from our OPO-based system. We measured the most probable beam velocity, 388 m/s. From this and the geometrical parameters presented in this section, we estimate the velocity component of the NO sample along the laser beam direction to be close to ±20 m/s. This leads to an estimate of the residual Doppler width, $\gamma_{\text{Doppler}}=190$ MHz. LIF is monitored about 10 cm from the nozzle by means of a solar-blind photomultiplier tube (PMT) (Hamamatsu Corp. R7154) and lens combination. The PMT signal is processed by a digital oscilloscope (LeCroy Corp. LT344) interfaced with a computer to generate the LIF spectra.

The narrow-band output of the OPO-based UV light source can be tuned to excite NO in either the $B\,^2\Pi_{1/2}$ $(v=3)\leftarrow X\,^2\Pi_{1/2}$ $(v=0)$ or $A\,^2\Sigma^+$ $(v=2)\leftarrow X\,^2\Pi_{1/2}$ $(v=0)$ band. Typical LIF spectra of lines in these bands are shown in Figs. 7 and 8, respectively. Both figures show spectral scans of about 3 GHz length. Scans of up to 15 GHz were also performed without mode hops from the diode laser. In Fig. 7, the R_{11} (0.5) rovibronic transition is shown. The spectrum shows clearly resolved Λ doublets and partially resolved hyperfine structure.[10] Gaussian functions are used to model the unresolved hyperfine substructure, allowing us to determine the observed linewidth of the molecular transitions, $\gamma_{\text{UVobserved,1}}=250$ MHz. The obtained average line position is approximately 0.15 cm^{-1} to the red from the value reported by Faris and Cosby.[51] This small difference is attributed to imprecise calibration of the wavemeter since the UV scale is calculated using the measured wavelengths from the scanning IR and (half) the Nd:YAG second harmonic. It is clear that further improvements to the absolute frequency calibration need to be implemented if one wishes to perform frequency metrology studies in the deep UV (e.g., Ref. 52).

Similarly, the data of Fig. 8 can also be used to obtain a second determination of this type. We accomplished this by comparing our spectra to simulations from the program

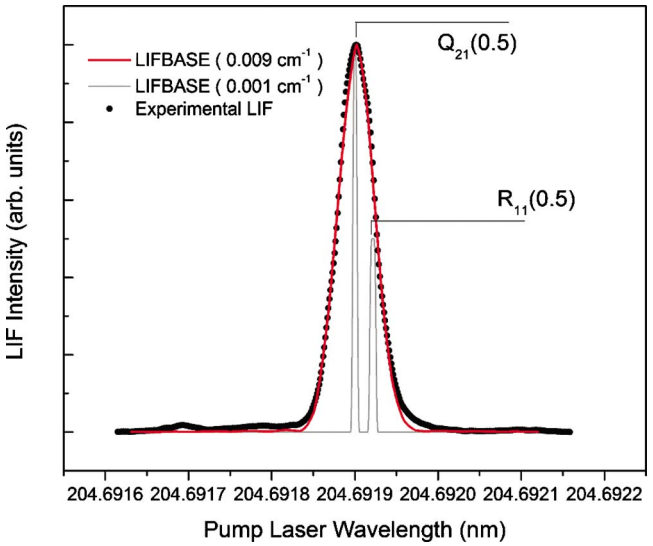

FIG. 8. (Color online) Typical LIF spectrum of the unresolved $R_{11}(0.5)Q_{21}(0.5)$ line pair of the $A\ ^2\Sigma^+\ (v=2) \leftarrow X\ ^2\Pi_{1/2}\ (v=0)$. The LIFBASE program (Ref. 53) was used to estimate the line broadening. Calculated spectra with total resolution of 0.009 cm^{-1} (270 MHz) (solid curve fit) and 0.001 cm^{-1} (30 MHz) (narrow doublet curve) are shown for evaluation of the UV source bandwidth and line assignment. The LIFBASE spectra were shifted by 0.188 cm^{-1} to the red to match the experimental curve.

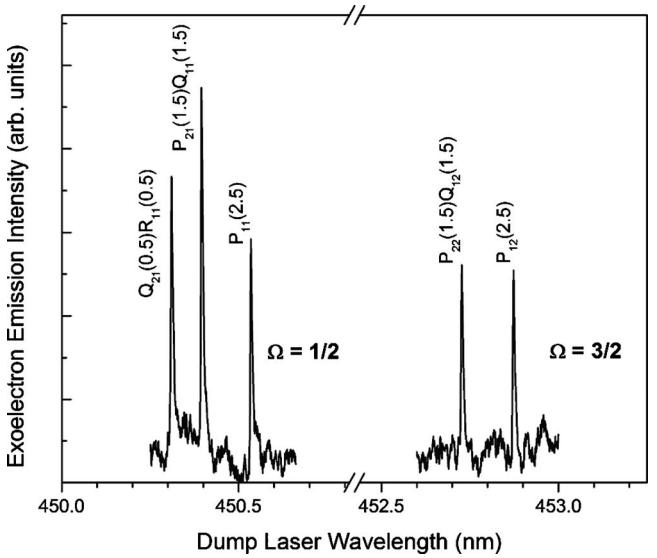

FIG. 9. Electron signal measured after the interaction of vibrationally excited NO ($v=16$) with a Au(111) surface with a submonolayer of Cs (see text). The unresolved $R_{11}(0.5)Q_{21}(0.5)$ line pair of the $A\ ^2\Sigma^+\ (v=2) \leftarrow X\ ^2\Pi_{1/2}\ (v=0)$ shown in Fig. 8 is used as the pump transition, while the DUMP laser is scanned. The group of lines on the left populate the $X\ ^2\Pi_{1/2}$, $v=16$, $\Omega=0.5$ rotational states while the group on the right corresponds to states with $X\ ^2\Pi_{1/2}$, $v=16$, $\Omega=1.5$.

LIFBASE (Ref. 53) for the unresolved $R_{11}(0.5)Q_{21}(0.5)$ line pair of the $A\ ^2\Sigma^+\ (v=2) \leftarrow X\ ^2\Pi_{1/2}\ (v=0)$ band. In this way, we find $\gamma_{\mathrm{UVobserved},2}=270$ MHz. We use the average of these two values, $\gamma_{\mathrm{UVobserved}}=260$ MHz, in further analysis below. We attribute the difference in bandwidth between the two measured lines to the change in wavelength of the OPO output. Saturation of the $A\ ^2\Sigma^+$ transitions was observed for pulse energies larger than $\sim 200\ \mu$J. When higher power is used the line intensity remains unchanged, the line broadens, and satellite lines attributed to otherwise negligible adjacent longitudinal cavity modes of the OPO appear in the spectrum spaced by one FSR in frequency space. Day-to-day operation showed excellent stability, with drifts on the order of only a few hundreds of megahertz prior to frequency locking of the pump and seed lasers.

While one obtains high spectral brightness with this light source, which is valuable for achieving efficient population transfer, spectral stability is also critical when carrying out experiments involving optical pumping. In such experiments, the population prepared by the laser must be reasonably stable, often over several hours in order that sufficient signal to noise may be obtained. A good example of an application that is rather demanding in this regard is stimulated emission pumping (SEP).[47,54–61] SEP is a folded variant of optical-optical double resonance that is particularly sensitive to wavelength instability due to the fact that the Λ transition is carried out between 2 ms or longer-lived vibrational states of the ground electronic state, whose natural linewidth is less than 1 kHz. Here a PUMP laser excites a molecule to a single rotational level of an excited electronic state and a second DUMP laser is used to stimulate emission transferring population back to a vibrationally excited level in the ground electronic state.

To transfer population from the vibrationless level of the NO molecule found in a molecular beam, the OPO-based UV light source is used to excite the PUMP transition $A\ ^2\Sigma^+\ (v=2) \leftarrow X\ ^2\Pi\ (v=0)$ shown in Fig. 8 and a DUMP laser tuned near 450 nm stimulates emission in the $A\ ^2\Sigma^+\ (v=2) \rightarrow X\ ^2\Pi\ (v=16)$ band. The DUMP laser system uses the third harmonic of a Nd:YAG laser (Spectra Physics PRO-200-10) to pump a dye laser (Sirah PRSC-DA-24) operating on Coumarin 450 generating pulses in the 430–470 nm region. The PUMP and DUMP laser beams are then overlapped in space and time with the molecular beam. To obtain the SEP spectra, we make use of vibrationally promoted electron emission to detect the population produced in $v=16$.[49,50,58] Here, a low work function (~ 1.6 eV) surface is produced by depositing ~ 0.5 ML Cs into a crystalline Au(111) surface. Electrons emitted from the surface are monitored while the PUMP wavelength is fixed on the $R_{11}(0.5)Q_{21}(0.5)$ transition, populating the $A\ ^2\Sigma^+\ (v=2)$ state and the DUMP wavelength is scanned. Figure 9 shows a series of sharp peaks corresponding to the allowed stimulated emission transitions to several rotational states of $X\ ^2\Pi\ (v=16)$, where the internal energy of the vibrationally excited NO molecules exceeds the solid's work function.

By achieving high stability and saturation of the PUMP transitions with our newly developed laser, the possibilities for added complexity of experiments involving vibrationally promoted exoelectrons are expanded. It is worth noticing that this system is well capable of producing light around 206 nm, which can be used to pump the a $^3\Pi\ (v=0) \leftarrow X\ ^1\Sigma^+\ (v=0)$ spin-forbidden Cameron band of CO. Metastable CO is an attractive molecule in particular for applications in Stark-deceleration experiments.[62]

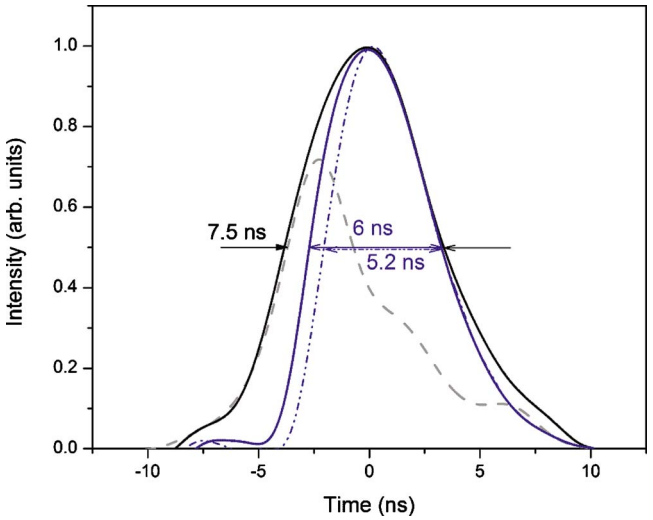

FIG. 10. (Color online) Time-averaged temporal profiles for the incident pump (broader solid curve), depleted pump output (dashed gray curve), and OPO signal (narrower solid curve). The peak height of the incident pump and signal are normalized to unit height, with the depleted pump left on the same scale as the pump pulse (pump depletion can be approximated as the difference of the two integrated areas). The unseeded signal (dot-dashed curve) is shown for comparison.

B. OPO characteristics

Figure 10 shows time resolved pulse shapes as obtained with a fast PD (Electro-Optics Technology ET-2000) for pump and signal beams of the OPO under seeded and unseeded operation. The injection-seeded signal output (narrower solid curve) shows a buildup time of approximately 1.5–2 ns, which is weakly dependent upon the pump laser power. In comparison, the unseeded pulses (double-dot-dashed curve) exhibit buildup times about 1 ns longer, corresponding roughly to one round trip time of the cavity. The injection seeding not only increases the intensity of the signal beam but it lengthens its pulse ($\Delta t \sim 6$ ns FWHM) due to the faster buildup time, which is also expected to improve the bandwidth. The FT limit for this signal transient shown in Fig. 10 in the idealized case of perfectly Gaussian-shaped pulses (i.e., $\Delta v \cdot \Delta t \sim 0.44$) restricts the bandwidth to $\Delta v \sim 73$ MHz.

Although the OPO signal's bandwidth was not directly measured, we may estimate it from other laboratory measurements, using the assumption that the bandwidths combine according to the sum of their squares,

$$\gamma_1^2 + \gamma_2^2 = \gamma_{1,2}^2 \tag{1}$$

for the sum frequency generation

$$\omega_1 + \omega_2 = \omega_{1,2}. \tag{2}$$

In this way one may show that

$$\gamma_{\text{signal}} = \frac{\gamma_{\text{UV}}}{\sqrt{5}}, \tag{3}$$

assuming $\gamma_{\text{signal}} \sim \gamma_{\text{idler}}$.

As was shown above, an upper bound of $\gamma_{\text{UVobserved}} = 260$ MHz was derived from UV LIF spectroscopy. Here the calculated maximum Doppler contribution, $\gamma_{\text{Doppler}} = 190$ MHz, must be removed (assuming Gaussian frequency profiles) as follows:

$$\gamma_{\text{UV}}^2 = \gamma_{\text{UVobserved}}^2 - \gamma_{\text{Doppler}}^2. \tag{4}$$

From this we derive an estimate of the Doppler-free UV bandwidth, $\gamma_{\text{UV}} = 177$ MHz, which leads to an estimate of the bandwidth for the IR signal output, $\gamma_{\text{signal}} \geq 79$ MHz, in line with the derived theoretical value above. This may be compared to an estimated bandwidth of ~100 MHz reported by Mahnke and co-workers.[29,63] Recently, Mahnke and Wirth[63] demonstrated that even when an OPO operates on a SLM, the linewidth might be broadened by the nondegenerate transversal modes. Additionally, shot-to-shot variations in the temporal profile and frequency chirp due to instantaneous variations in output frequency during the pulse may further increase the optical bandwidth.[37,38,64] Chirp effects are minimized by reducing the pump energy and keeping the free-running wavelength of the phase-matched OPO as close as possible to the seeding wavelength.

We also obtained experimentally derived information on the efficiency of specific key wavelength conversion steps in the OPO-based system. In particular, we obtained the ratio of the signal to pump photon number (N), which is the OPO's quantum efficiency,

$$\varepsilon_q = \frac{N_{\text{signal}}}{N_{\text{pump}}}, \tag{5}$$

in two ways. First, using a laser energy meter (Gentec Electro-Optics, Inc.) we measured the pump beam depletion by tuning the KTP crystals to and away from their phase matching angles. The obtained quantum efficiency was $\varepsilon_q \sim 0.4$ at large pump powers. Second, we measured the pump-signal energy conversion efficiency,

$$\frac{I_{\text{signal}}}{I_{\text{pump}}} = 0.23, \tag{6}$$

and corrected for the difference in pump and signal photon energies,

$$\frac{I_{\text{signal}}\lambda_{\text{pump}}}{I_{\text{pump}}\lambda_{\text{signal}}} = 0.23\frac{532 \text{ nm}}{914 \text{ nm}} = 0.4. \tag{7}$$

Results of more comprehensive measurements as a function of pump energy are shown in Fig. 11. Here, one can see that ε_q rises rapidly from the oscillation threshold and more slowly above a pump energy of ~60 mJ/pulse. Nevertheless ε_q continues to climb even up to the highest pump energies used in this work. Measurements without seeding are also shown for comparison, where one can clearly observe a higher oscillation threshold and reduced quantum efficiency.[65]

We also examined the sum frequency conversion step used to generate the deep-UV light both by computer modeling (using the SNLO program) and experimentally. Due to the tight constraints on angular and bandwidth acceptance set by phase matching conditions in the nonlinear mixing crystal,[66] a high-efficiency SFG process requires beams with low divergence and nearly identical spatial properties in addition to narrow linewidths with optimum spectral and tem-

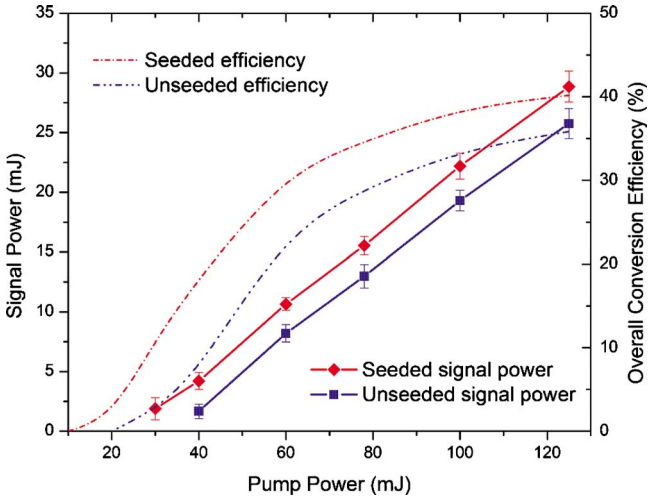

FIG. 11. (Color online) Average output energy/pulse measured for the signal beam and overall conversion efficiency (measured by pump depletion) for seeded and unseeded oscillation plotted vs forward pump energy.

poral overlap. These requirements are often difficult to obtain in high power nanosecond light sources, especially when using dyes as the gain medium.

As mentioned above, the injection-seeding technique of this work leads to significantly improved beam quality and reduced divergence while producing near FT-limited pulses. This alone brings us closer to the aforementioned requirements for more efficient SFG. Furthermore, the buildup time is typically reduced by about 1 ns upon injection seeding as shown in Fig. 10, increasing the pulse duration and therefore improving the temporal overlap (with low pulse-to-pulse temporal jitter) with the fourth-harmonic pulse of the Nd:YAG laser in the mixing crystal.

The routinely obtained efficiency for the mixing of narrow bandwidth near-IR pulses with the fourth harmonic of the injection-seeded pump laser in a 1 cm long BBO crystal was ~30%. For example, with 60 mJ/pulse in ω_{pump} (at 532 nm) we routinely obtained 14 mJ/pulse in ω_{signal} (at 919 nm), which when mixed with 10 mJ of 266 nm light yielded 3–4 mJ at 206 nm (25%–34% conversion efficiency). The 266 nm pulse energy was kept below 10 mJ to avoid damage to the BBO crystal. It should be noted that higher energies are possible, but one must pay careful attention to all other factors that contribute to crystal damage. Specifically, with this laser system, pulse energies of up to 5 mJ in the deep UV were obtained; however a slow degradation of the BBO mixing crystal's polished surfaces was observed over a period of several months of operation, limiting the maximum power obtained. Heating of the BBO to avoid water vapor deposition at the polished surfaces or purging the crystal environment with dry N_2 will, in all likelihood, help to reduce this problem.

An alternative configuration consists of splitting the 532 nm beam from the injection-seeded Nd:YAG laser into two beams, one acting as the OPO pump and the other as the pump source for the fourth harmonic generation. In this way, any degradation of the OPO pump beam quality (and related OPO performance) by the generation of the fourth harmonic is avoided and also the amount of 266 nm light generated is reduced, therefore minimizing potential optical damage to the SFG crystal (see for example Ref. 67).

It is worth mentioning that calculations using the SNLO program show that by using a cesium lithium borate ($CsLiB_6O_{10}$ or CLBO) crystal for sum frequency mixing of the idler beam of our OPO (set at ~1.27 μm) with the fifth harmonic of the Nd:YAG laser (213 nm), wavelengths as short as 182.5 nm can be obtained.

IV. SUMMARY

We have implemented a novel all-solid-state source of tunable deep-UV radiation capable of generating up to 5 mJ/pulse with a bandwidth better than 0.01 cm^{-1}. The UV output is produced by highly efficient sum frequency generation of FT-limited near-IR pulses and the fourth harmonic beam of an injection-seeded Nd:YAG laser. The high conversion efficiency of this process was measured to be ~30% and is attributed to the good quality of the near-IR beam. This narrowband light is produced by injection seeding of a home-built dual KTP crystal OPO which has an overall conversion efficiency of >40%. The injected cw seeding light originated from an external cavity diode laser is tunable between 875 and 940 nm. The OPO cavity was actively stabilized to the diode wavelength by a new computer-controlled variant of the intensity-dip locking method. The UV tuning range was 204–207, limited by the diode laser. This range can be easily extended by exchanging first the laser diode (202–210 nm), and then the cavity mirrors and KTP crystals if necessary (to a total range of ~190–212 nm). Also by using the idler of our current configuration (~1.27 μm) and the fifth harmonic of the Nd:YAG laser, wavelengths lower than 185 nm can be achieved in a CLBO mixing crystal.

ACKNOWLEDGMENTS

This work is supported by the National Science Foundation (Grant No. CHE0724038). We are grateful to Peter Mahnke (Institute of Technical Physics, Stuttgart, Germany) for many helpful suggestions on the implementation of the OPO and his comments on the draft of this manuscript. L.V. thanks the support from the University of California President's Postdoctoral Fellowship.

[1] G. W. Baxter, M. A. Payne, B. D. W. Austin, C. A. Halloway, J. G. Haub, Y. He, A. P. Milce, J. Nibler, and B. J. Orr, Appl. Phys. B: Lasers Opt. **71**, 651 (2000).
[2] W. D. Kulatilaka, T. N. Anderson, T. L. Bougher, and R. P. Lucht, Appl. Phys. B: Lasers Opt. **80**, 669 (2005).
[3] M. Drabbels, S. Stolte, and G. Meijer, Chem. Phys. Lett. **200**, 108 (1992).
[4] J. M. Price, A. Ludviksson, M. Nooney, M. Xu, R. M. Martin, and A. M. Wodtke, J. Chem. Phys. **96**, 1854 (1992).
[5] M. Drabbels, C. G. Morgan, D. S. McGuire, and A. M. Wodtke, J. Chem. Phys. **102**, 611 (1995).
[6] C. G. Morgan, M. Drabbels, and A. M. Wodtke, J. Chem. Phys. **104**, 7460 (1996).
[7] C. G. Morgan, M. Drabbels, and A. M. Wodtke, J. Chem. Phys. **105**, 4550 (1996).
[8] E. Cromwell, T. Trickl, Y. T. Lee, and A. H. Kung, Rev. Sci. Instrum. **60**, 2888 (1989).
[9] H. Zuckermann, Y. Haas, M. Drabbels, J. Heinze, W. L. Meerts, J. Reuss, and J. Vanbladel, Chem. Phys. **163**, 193 (1992).

[10] M. Drabbels and A. M. Wodtke, Chem. Phys. Lett. **256**, 8 (1996).
[11] W. Ubachs, K. S. E. Eikema, W. Hogervorst, and P. C. Cacciani, J. Opt. Soc. Am. B **14**, 2469 (1997).
[12] U. Hollenstein, H. Palm, and F. Merkt, Rev. Sci. Instrum. **71**, 4023 (2000).
[13] M. Sneep, S. Hannemann, E. J. van Duijn, and W. Ubachs, Opt. Lett. **29**, 1378 (2004).
[14] S. Hannemann, E. J. van Duijn, and W. Ubachs, Rev. Sci. Instrum. **78**, 103102 (2007).
[15] T. A. Paul and F. Merkt, J. Phys. B **38**, 4145 (2005).
[16] J. A. J. Fitzpatrick, O. V. Chekhlov, J. M. F. Elks, C. M. Western, and S. H. Ashworth, J. Chem. Phys. **115**, 6920 (2001).
[17] D. J. Armstrong and A. V. Smith, IEEE J. Sel. Top. Quantum Electron. **13**, 721 (2007).
[18] T. K. Minton, S. A. Reid, H. L. Kim, and J. D. McDonald, Opt. Commun. **69**, 289 (1989).
[19] W. R. Bosenberg and D. R. Guyer, J. Opt. Soc. Am. B **10**, 1716 (1993).
[20] J. Mes, W. Hogervorst, and V. Tugbaev, Opt. Commun. **196**, 229 (2001).
[21] A. Fix and G. Ehret, Appl. Phys. B: Lasers Opt. **67**, 331 (1998).
[22] D. C. Hovde, J. H. Timmermans, G. Scoles, and K. K. Lehmann, Opt. Commun. **86**, 294 (1991).
[23] C. E. Hamilton and W. R. Bosenberg, *Conference on Lasers and Electro-Optics* (Optical Society of America, Washington, DC, 1992), Vol. 12, pp. 370–371.
[24] A. V. Smith, W. J. Alford, T. D. Raymond, and M. S. Bowers, J. Opt. Soc. Am. B **12**, 2253 (1995).
[25] M. J. T. Milton, T. D. Gardiner, F. Molero, and J. Galech, Opt. Commun. **142**, 153 (1997).
[26] O. Votava, J. R. Fair, D. F. Plusquellic, E. Riedle, and D. J. Nesbitt, J. Chem. Phys. **107**, 8854 (1997).
[27] G. Ehret, A. Fix, V. Weiss, G. Poberaj, and T. Baumert, Appl. Phys. B: Lasers Opt. **67**, 427 (1998).
[28] A. V. Smith and D. J. Armstrong, J. Opt. Soc. Am. B **19**, 1801 (2002).
[29] P. Mahnke, H. H. Klingenberg, A. Fix, and M. Wirth, Appl. Phys. B: Lasers Opt. **89**, 1 (2007).
[30] Y. He and B. J. Orr, Appl. Phys. B: Lasers Opt. **96**, 545 (2009).
[31] Y. He, G. W. Baxter, and B. J. Orr, Rev. Sci. Instrum. **70**, 3203 (1999).
[32] D. J. Armstrong, W. J. Alford, T. D. Raymond, A. V. Smith, and M. S. Bowers, J. Opt. Soc. Am. B **14**, 460 (1997).
[33] This coating is a single MgF_2 layer that protects the polished surface from fogging due to ambient moisture.
[34] SNLO nonlinear optics code available from A. V. Smith (AS-Photonics, Albuquerque, NM).
[35] D. J. Armstrong, W. J. Alford, T. D. Raymond, and A. V. Smith, Appl. Opt. **35**, 2032 (1996).
[36] M. Wirth, A. Fix, P. Mahnke, H. Schwarzer, F. Schrandt, and G. Ehret, Appl. Phys. B: Lasers Opt. **96**, 201 (2009).
[37] R. T. White, Y. B. He, B. J. Orr, M. Kono, and K. G. H. Baldwin, Opt. Lett. **28**, 1248 (2003).
[38] R. T. White, Y. He, B. J. Orr, M. Kono, and K. G. H. Baldwin, J. Opt. Soc. Am. B **24**, 2601 (2007).
[39] E. S. Cassedy and M. Jain, IEEE J. Quantum Electron. **15**, 1290 (1979).
[40] G. Anstett and R. Wallenstein, Appl. Phys. B: Lasers Opt. **79**, 827 (2004).
[41] T. W. Hansch and B. Couillaud, Opt. Commun. **35**, 441 (1980).
[42] R. W. P. Drever, J. L. Hall, F. V. Kowalski, J. Hough, G. M. Ford, A. J. Munley, and H. Ward, Appl. Phys. B: Photophys. Laser Chem. **31**, 97 (1983).
[43] R. L. Schmitt and L. A. Rahn, Appl. Opt. **25**, 629 (1986).
[44] K. Ertel, H. Linne, and J. Bosenberg, Appl. Opt. **44**, 5120 (2005).
[45] See supplementary material at http://dx.doi.org/10.1063/1.3436973 for the LabVIEW™ program developed to lock the OPO cavity to the injection seed laser.
[46] S. Kobtsev, S. Kandrushin, and A. Potekhin, Appl. Opt. **46**, 5840 (2007).
[47] M. Drabbels, A. M. Wodtke, M. Yang, and M. H. Alexander, J. Phys. Chem. A **101**, 6463 (1997).
[48] J. Chen, D. Matsiev, J. D. White, M. Murphy, and A. M. Wodtke, Chem. Phys. **301**, 161 (2004).
[49] J. D. White, J. Chen, D. Matsiev, D. J. Auerbach, and A. M. Wodtke, J. Vac. Sci. Technol. A **23**, 1085 (2005).
[50] J. D. White, J. Chen, D. Matsiev, D. J. Auerbach, and A. M. Wodtke, J. Chem. Phys. **124**, 064702 (2006).
[51] G. W. Faris and P. C. Cosby, J. Chem. Phys. **97**, 7073 (1992).
[52] S. Hannemann, E. J. Salumbides, S. Witte, R. T. Zinkstok, E. J. van Duijn, K. S. E. Eikema, and W. Ubachs, Phys. Rev. A **74**, 062514 (2006).
[53] J. Luque and D. R. Crosley, SRI International Report No. MP 99–009, 1999.
[54] C. E. Hamilton, J. L. Kinsey, and R. W. Field, Annu. Rev. Phys. Chem. **37**, 493 (1986).
[55] C. Kittrell, E. Abramson, J. L. Kinsey, S. A. McDonald, D. E. Reisner, R. W. Field, and D. H. Katayama, J. Chem. Phys. **75**, 2056 (1981).
[56] X. M. Yang, E. H. Kim, and A. M. Wodtke, J. Chem. Phys. **96**, 5111 (1992).
[57] M. Drabbels and A. M. Wodtke, J. Chem. Phys. **106**, 3024 (1997).
[58] N. H. Nahler, J. D. White, J. Larue, D. J. Auerbach, and A. M. Wodtke, Science **321**, 1191 (2008).
[59] Y. H. Huang, C. T. Rettner, D. J. Auerbach, and A. M. Wodtke, Science **290**, 111 (2000).
[60] J. D. White, J. Chen, D. Matsiev, D. J. Auerbach, and A. M. Wodtke, Nature (London) **433**, 503 (2005).
[61] A. M. Wodtke, Y. H. Huang, and D. J. Auerbach, J. Chem. Phys. **118**, 8033 (2003).
[62] H. L. Bethlem, G. Berden, and G. Meijer, Phys. Rev. Lett. **83**, 1558 (1999).
[63] P. Mahnke and M. Wirth, Appl. Phys. B: Lasers Opt. **99**, 141 (2010).
[64] M. Kono, K. G. H. Baldwin, Y. B. He, R. T. White, and B. J. Orr, J. Opt. Soc. Am. B **23**, 1181 (2006).
[65] The bandwidth of the unseeded OPO was measured to be about 5–8 cm^{-1}.
[66] Preliminary calculations using cesium lithium borate ($CsLiB_6O_{10}$ or CLBO) show promising properties for our UV applications when mixing near-IR with the fourth harmonic of the Nd:YAG laser. CLBO is transparent down to 190 nm and has much larger (e.g., 18 times at 919 +266 nm) angular and spectral bandwidths than BBO. Although it has a slightly lower d_{eff} than BBO, the walkoff angle is much smaller (~17 times at these wavelengths) and the damage threshold is larger than BBO by about a factor of 2. Note that only wavelengths longer than 915 nm fulfill the phase matching conditions for mixing with 266 nm light, limiting the tunability the region to >206 nm.
[67] A. Mesiter, Ph.D. thesis, University of Bayreuth, 2005.